Biomed Microdevices (2015) 17:29
DOI 10.1007/s10544-015-9935-z

Enhanced sub-micron colloidal particle separation with interdigitated microelectrode arrays using mixed AC/DC dielectrophoretic scheme

Vikhram V. Swaminathan · Mark A. Shannon · Rashid Bashir

Abstract Dielectrophoretic separation of particles finds a variety of applications in the capture of species such as cells, viruses, proteins, DNA from biological systems, as well as other organic and inorganic contaminants from water. The ability to capture particles is constrained by poor volumetric scaling of separation force with respect to particle diameter, as well as the weak penetration of electric fields in the media. In order to improve the separation of sub-micron colloids, we present a scheme based on multiple interdigitated electrode arrays under mixed AC/DC bias. The use of high frequency longitudinal AC bias breaks the shielding effects through electroosmotic micromixing to enhance electric fields through the electrolyte, while a transverse DC bias between the electrode arrays enables penetration of the separation force to capture particles from the bulk of the microchannel. We determine the favorable biasing conditions for field enhancement with the help of analytical models, and experimentally demonstrate the improved capture from sub-micron colloidal suspensions with the mixed AC/DC electrostatic excitation scheme over conventional AC-DEP methods.

Keywords Interdigitated electrodes · Dielectrophoresis · Colloidal particle · Particle separation · Microfluidics

Dedicated to the memory of (late) Prof. Mark A Shannon.

V. V. Swaminathan · M. A. Shannon
Department of Mechanical Science and Engineering, University of Illinois at Urbana-Champaign, 1206 West Green Street, Urbana, IL 61801, USA

V. V. Swaminathan · R. Bashir
Micro and Nanotechnology Laboratory, University of Illinois at Urbana-Champaign, 208 North Wright Street, Urbana, IL 61801, USA

R. Bashir
Department of Electrical and Computer Engineering, University of Illinois at Urbana-Champaign, 306 North Wright Street, Urbana, IL 61801, USA

R. Bashir (✉)
Department of Bioengineering, University of Illinois at Urbana-Champaign, 1270 Digital Computer Laboratory MC-278, 1304 West Springfield Avenue, Urbana, IL 61801, USA
e-mail: rbashir@illinois.edu

Published online: 15 February 2015

1 Introduction

Dielectrophoresis (DEP) is based on the separation of neutral particles that are polarized under a spatially non-uniform electric field (Pohl 1978). Over the years, this method has gained considerable interest (Pethig 2010) in the separation of biological species, and DEP has been demonstrated widely for capture, segregation and even patterning of rare cells, bacteria, viruses and other biomolecules (Bajaj et al. 2013; Čemažar et al. 2011; Cen et al. 2004; Gadish and Voldman 2006; Huang et al. 2013; Li et al. 2005; Park et al. 2007, 2009; Pratt et al. 2011; Zhu et al. 2010). The time-averaged DEP forces acting on a particle is given by (Gascoyne and Vykoukal 2002; Liu and Garimella 2009)

$$\left\langle \overrightarrow{F_E}(t) \right\rangle = 2\pi\varepsilon_m r^3 \left\{ \mathrm{Re}(K(\omega))\nabla E_{RMS}^2 + \mathrm{Im}(K(\omega)) \left(E_x^2\nabla\varphi_x + E_y^2\nabla\varphi_y + E_z^2\nabla\varphi_z \right) \right\} \quad (1)$$

Where, r is the radius of the particle, ε_m is the electric permittivity of the medium, $\overrightarrow{E}$ is the applied electric field, φ_i (i=x,y,z), its spatial phase components, and $K(\omega)$ is

the frequency dependent Clausius-Mossotti factor that determines the nature of DEP forces (see appendix). The two components described on the right-hand side of Eq. (1) describe the DEP (real) and travelling wave (twDEP - imaginary) effects respectively. DEP efficiency scales poorly due to the volumetric dependence on the particle size and, further, it is also inversely dependent on the spatial dimensions of the system (Albrecht et al. 2004; Cao et al. 2008). Hence the forces are weak compared to thermal fluctuations to cause separation of sub-micron sized colloids (Castellanos et al. 2003). Various approaches have been adopted for enhancing the DEP effects such as with the use interdigitated electrode arrays and traveling wave schemes (Edwards et al. 2009; Jo et al. 2012; Li et al. 2004; Sun et al. 2007; Yantzi et al. 2007), multiple frequency DEP (Wang et al. 2009) and novel electrode shape/topology effects (Gadish and Voldman 2006; Horii et al. 2014; Pratt et al. 2011; Yasukawa et al. 2012). However, the electric field typically decays rapidly towards the bulk away from the electrodes, and hence the DEP effects are weaker in these regions. In this paper, we present a mixed AC/DC excitation scheme using two pairs of interdigitated electrode arrays in a longitudinal AC bias and a transverse DC bias that collectively enable enhanced separation of the colloids from the bulk. The method draws its advantages from the AC electroosmosis induced micromixing effects that break the shielding effects (Bazant and Squires 2010; Pascall and Squires 2010; Ramos et al. 1999; Sun et al. 2007; Wu 2008; Zhou et al. 2005) to enable further penetration of the separation forces in the bulk region of the microchannel.

A schematic of the colloid separation method is depicted in Fig. 1a. The device consists of two pairs of interdigitated microelectrodes patterned on either side of a microfluidic channel. Using a mixed AC/DC biasing scheme, it is possible to establish enhanced separation fields that cause particles in the flow to collect over the electrodes. Figure 1b shows the biasing method. Each pair of interdigitated electrode is in longitudinal high-frequency AC bias. At the same time, a transverse bias is applied across the channel by providing a DC offset for one pair of electrodes relative to the second pair. The power sources that drive both these electrode pairs are connected in-phase to control the uniformity of the transverse signal. At high frequency, the AC bias perturbs the vicinity of the electrodes so fast so as to prevent salt ions from accumulating in the EDL, through electroosmotic pumping (Fig. 1c). The magnitudes of the AC and DC components are adjusted in such a way as to ensure maximum electroosmotic depolarization, while the transverse field is simultaneously maintained for improved separation. Figure 1d shows a micrograph of a device with two pairs of electrodes embedded underneath a 100 nm thin Si_3N_4 dielectric in a microchannel, prior to the final bonding of the PDMS microfluidic layer. The electrodes in each pair are 5 μm wide and 5 μm apart. Across the channel, electrode lengths are 50 μm and the gap between both pairs is 50 μm.

2 Theory

DC electrostatic fields are ineffective for separation in aqueous suspensions because of rapid shielding by counter-ions that migrate towards the electrodes to form the electrochemical double layers (EDLs) that shield their surface potential (Bard and Faulkner 2001). When AC electrostatics is incorporated, however, the RC-constant of the EDL determines the effectiveness of the ion shielding. At low frequencies, similar to the DC biasing case, the ions migrate rapidly and shield the

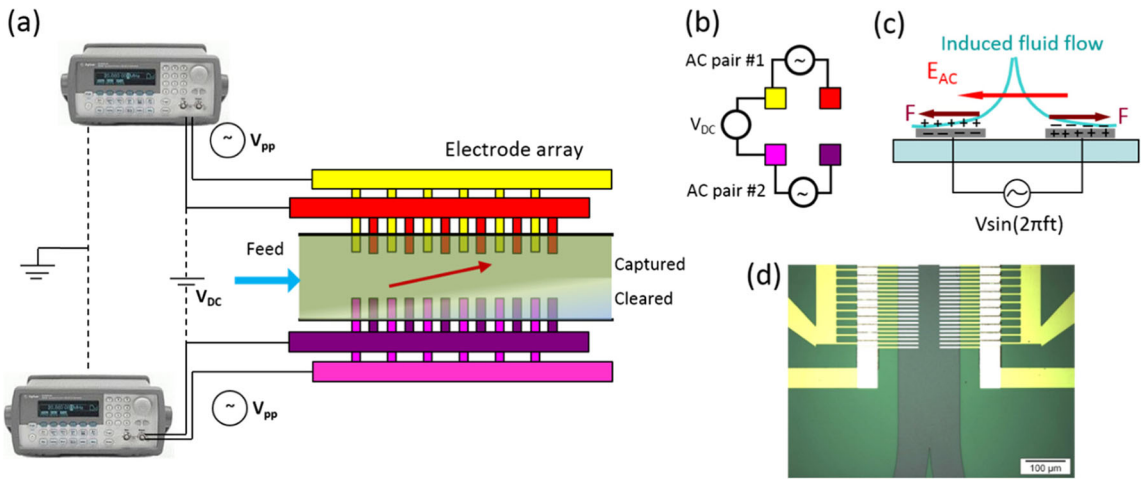

Fig. 1 Schematic of the AC/DC combined separation method. **a** Layout of the experimental setup showing two arrays of interdigitated electrodes in mixed AC/DC excitation to cause improved colloidal separation. **b** Shows the excitation scheme where each electrode (*color-coded*) is in lengthwise AC bias, with a transverse DC offset across the channel between electrode pairs. **c** Schematic of AC electroosmotic flow that occurs over the interdigitated electrodes to break EDL formation and sustain electric field in bulk. **d** Micrograph of a device with pairs of interdigitated electrodes, prior to PDMS channel attachment

electrodes. When the frequency approaches the RC-characteristic of the electrodes, this causes perturbation of the ions which are then forced to circulate locally around the electrodes due to the phenomenon of electroosmotic pumping. As a result, the induced electroosmotic flow causes chaotic mixing around the electrodes and prevents the formation of EDL—thus decreasing the potential drop across the EDL. Electric fields now penetrate out into the bulk electrolyte and the colloidal particles can experience the forces to be separated out.

Ramos et al., have provided an elegant analytical model for determining the electroosmotic depolarization by micromixing around interdigitated electrodes (Pascall and Squires 2010; Ramos et al. 1999). The local electric field lines around the microelectrodes follow semi-circular paths and can be modeled as a parallel circuit of infinitesimal current tubes flowing through two linearized EDL capacitors in series with a solution resistance. The voltage drop, V_{Debye}, in the EDL, as a function of the peak-to-peak bias, V_{PP}, and the electrode width/spacing, z, is given by

$$V_{Debye} = \frac{V_{PP}}{2}\frac{1}{(1+j\Omega)} \tag{2}$$

where, $\Omega = \omega\frac{\pi}{2}\frac{\varepsilon_m}{\sigma_m}\frac{z}{\lambda_D}$, λ_D, the Debye length, ω the angular frequency and σ_m is the conductivity of the medium. The time averaged electroosmotic velocity, <v>at the electrodes is given by

$$\langle v\rangle = \frac{\varepsilon_m V_{PP}^2 \Omega^2}{8\eta z\left(1+\Omega^2\right)^2} \tag{3}$$

where, η is the dynamic viscosity of the medium.

Figure 2 shows of the effects of AC electric field induced electroosmotic flow in overcoming the EDL shielding. The relative potential drop due to ionic shielding, V_{Debye}/V_{PP}, (Fig. 2a) has been determined by the circuit analysis model in Eq. (2). While most of the potential drop occurs within the EDL at low frequencies, the effect of the AC induced electroosmotic flow becomes apparent at intermediate and higher frequencies (≥1 kHz). This can also be seen in Fig. 2b where the mean electroosmotic velocity (by solving Eq. (3)) at the electrodes increases at these frequencies to its maximum value and finally decreases to zero again because the AC cycling is too fast for the ions to follow. When $f_{AC} \geq {}^{1}/_{RC}$, the EDL capacitance is completely disrupted by the micromixing and hence $V_{Debye} \rightarrow 0$. Under this condition, all of the applied voltage extends out to the bulk solution, where the colloids may be perturbed. The curves in Fig. 2a and b shift towards higher frequencies as the electrode dimensions decrease in size. However, the corresponding electric field strength is much higher because it inversely scales with the length. This is advantageous for increasing the force of separation acting on the particles. Figure 2c shows plots of V_{Debye}/V_{PP} for various ionic strength media. The threshold frequency for electroosmotic field enhancement increases with the salt concentration due to the decreased RC-constant as the Debye length decreases.

The electric field distribution under the combined AC-DC biasing scheme was simulated computationally (Fig. 3) using a finite element solver in Comsol Multiphysics 4.4®. The domain consisted of two pairs of electrodes, each made of 5 μm wide electrodes with 5 μm spacing, set 100 μm apart. The lengthwise high-aspect ratio of these electrodes (≥20:1), and large center-to-center distance (100 μm) between the pairs compared to the electrode width enabled simplifying the system to a 2-D model domain. A 0.1 μm thin Si_3N_4 dielectric (ε_r=7) was incorporated as a passivation layer over the electrodes, which were set to their respective biasing potentials of 2 V_{PP} AC longitudinal and 1 V DC transverse bias, and the channel region was composed of a aqueous dielectric (ε_r=80). Physical continuity at the interface between the dielectrics was enforced by maintaining compatibility between the displacement electric fields ($\vec{D} = \varepsilon_r\varepsilon_0\vec{E}$) on either side, while a periodic boundary condition was applied on the transverse walls of the domain to ensure continuity of electric flux.

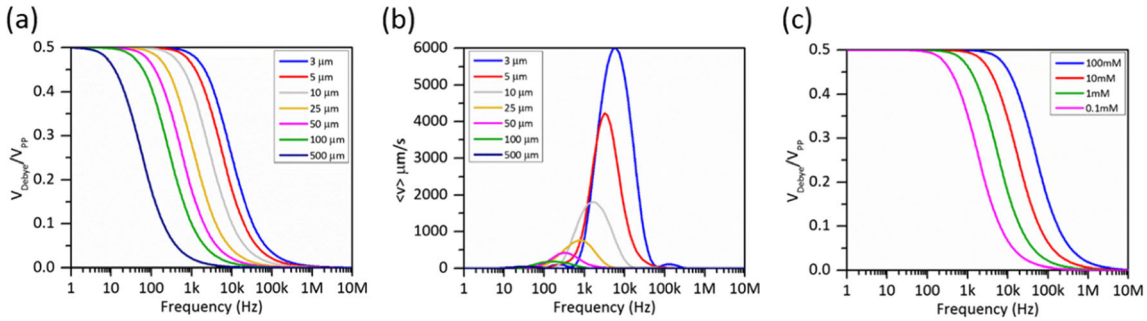

Fig. 2 Calculations of AC electroosmotic flow parameters while breaking the EDL barrier. **a** Normalized potential drop in the capacitive EDL compared to the resistive bulk vs. frequency for various electrode dimensions. **b** Time-averaged electroosmotic velocity in the EDL vs. frequency for various electrode dimensions. <v>is maximized at Ω=1 and<v>→ 0 as V_{Debye} approaches 0. **c** Normalized voltage drop in EDL vs. frequency for 5 μm electrodes across various salt concentrations. As salt content increases, the curve shifts towards higher AC frequency

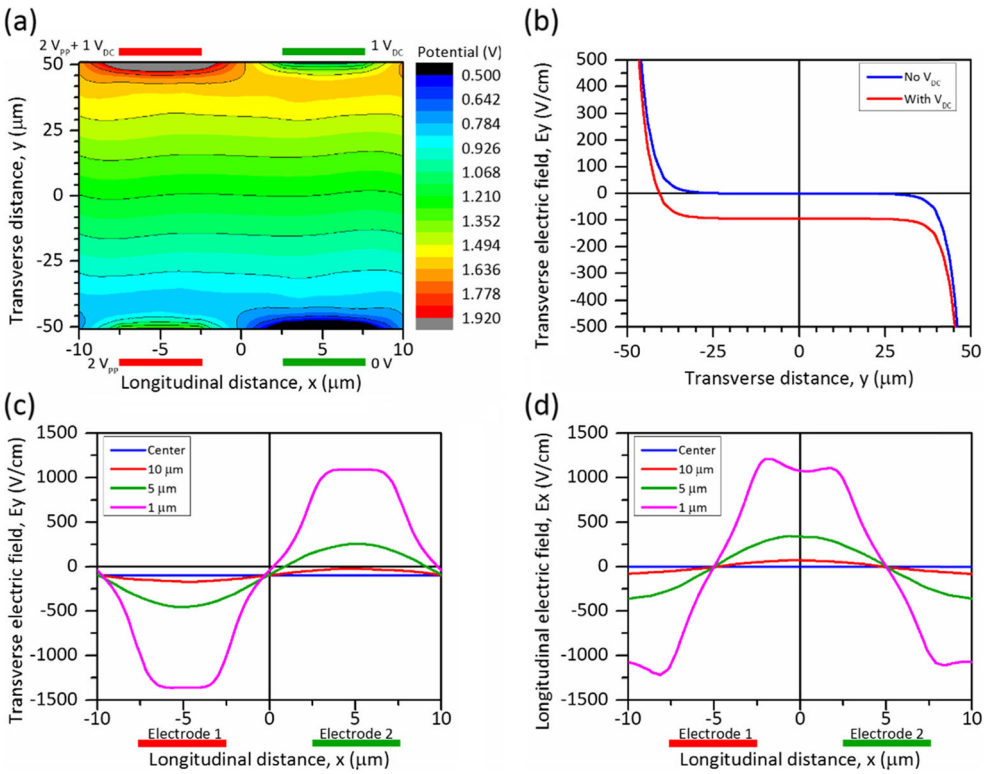

Fig. 3 Computational solution (RMS) of the potential and electric field distributions using our biasing scheme. **a** Potential distribution in the channel when a 2 V_{PP} AC excitation is used along with transverse 1 V DC bias. **b** Transverse electric field, E_y, across the channel on a section through the electrodes, with and without the transverse bias. **c** Transverse and **d** longitudinal electric fields along various cross-sections parallel to the channel. The relative location of electrodes in **a**, **c** and **d** is also shown schematically

Considering high-frequency depolarization, the EDL capacitive effects were ignored, as were other effects such as electrothermal heating and flow induced charge separations.

Figure 3a shows the root-mean-squared (RMS) potential distribution in the channel. Due to high-frequency depolarization, it is possible to sustain a transverse gradient that aids in colloid separation. Partial asymmetry also arises in the solution due to this transverse bias across the channel, which is seen in Fig. 3c and d. Figure 3b shows a comparison of the transverse electric field, E_y, across the channel, with and without the transverse bias. When only a conventional AC bias is used, the electric field decays within ca. 10 μm from the electrodes at either side of the channel and hence particles in the bulk will be unperturbed. However, under the mixed biasing scheme, it is possible to sustain as high as 100 V/cm in the transverse potential gradient. Figures 3c and d show the respective transverse (E_y) and longitudinal (E_x) components of the electric field along various sections of the channel. Within the proximity of the electrodes (1–5 μm), high field intensity (500–1500 V/cm) leads to the electroosmotic depolarization and also provides large trapping forces near the electrodes. As expected, the transverse electric field is maximum directly above the center of the electrodes, but the longitudinal component is maximized at the electrode edges. While the field decays to less than 10 % of the peak value at 10 μm, we are still able to sustain 100 V/cm in E_y as E_x is practically zero in the bulk region. Furthermore, using the mixed scheme, we can sustain a non-zero electric field profile across the channel and at least 10-fold larger gradients that are necessary in the proximity of the electrodes to overcome EDL shielding.

3 Experimental

3.1 Microfabrication steps

Figure 4 shows a step-by-step fabrication sequence for the microfluidic colloid separation device. The substrate used is a 500 μm thick silicon wafer with 1 μm thick LPCVD silicon nitride that provides complete electrical isolation. Interdigitated electrodes are patterned through conventional photolithography of a bilayer photoresist combination of lift-off resist LOR3A and photosensitive Shipley S1805 in step a. This is followed by e-beam evaporation of 100 nm thick of Ti/Pt and lift-off to reveal the electrodes in step b. A 400 nm thick dielectric layer of PECVD Si_3N_4 is deposited to cover the electrodes and passivate the metal surface from Faradaic reactions at high applied bias. In step c, vias in the Si_3N_4 layer are isotropically etched using Freon RIE to reveal openings on the second electrode of each pair. This step uses a 100 nm thick Cr/Cu lift-off

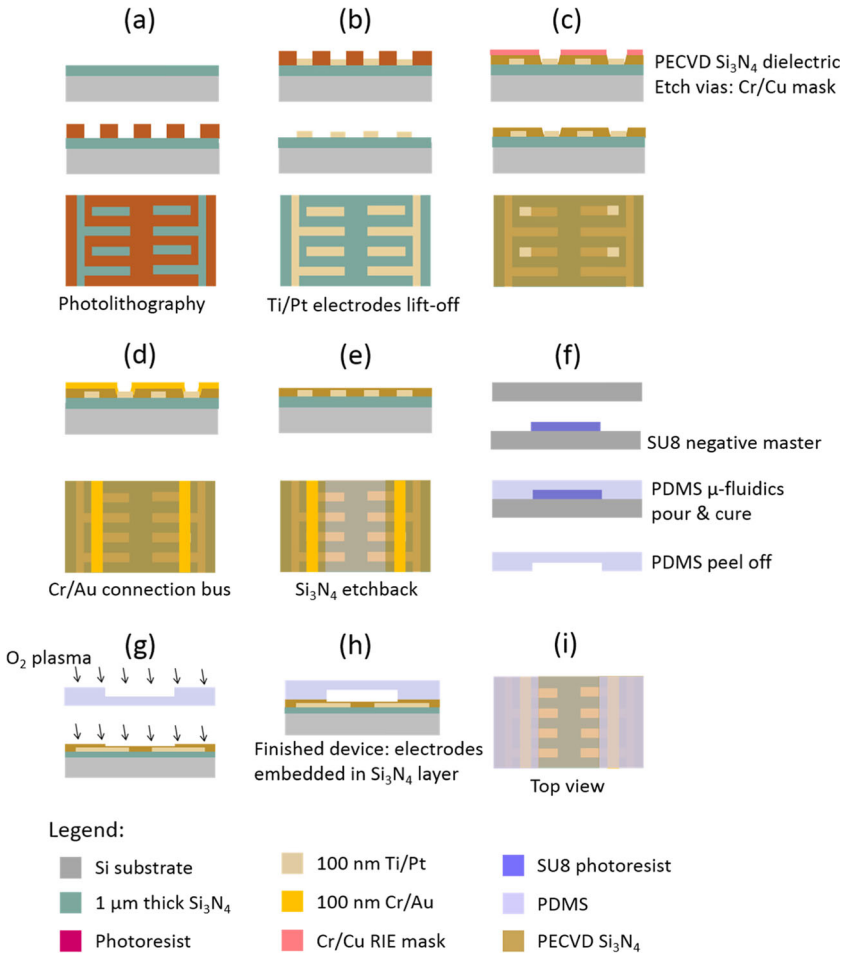

Fig. 4 Fabrication steps for the microfluidic colloid separation device. **a** Photolithography. **b** Lift-off pattern Cr/Au/Cr electrodes 100 nm thick. **c** Deposit 400 nm thick PECVD Si_3N_4 and pattern vias using CF_4 RIE with Cu sacrificial mask. **d** Deposit and pattern Cr/Au connection bus (100 nm thick) for 2nd electrodes. **e** CF_4 RIE thinning of dielectric over the electrodes. **f** Pattern SU-8 channel template, PDMS molding & peel off for channels. **g** O_2 plasma for channel bonding. **h** Irreversible PDMS-Si_3N_4 bonding with alignment of channel/electrodes. **i** Final top view assembly showing a cut section through PDMS

patterned layer as the etch mask. Subsequently, a 100 nm thick Cr/Au connection bus is deposited and patterned on either side to complete the connections. Steps c and d are crucial for the electrical connections, while maintaining electrical isolation between the electrodes within each pair. In step e, the Si_3N_4 dielectric is thinned down over the electrodes to <200 nm in the microchannel region using the Freon RIE. The microfluidic layer is fabricated out of PDMS in step f. A 25 μm thick SU8 master template of the microchannel is patterned using SU8-25 on a 500 μm thick bare silicon wafer. A degassed mix of Sylgard® PDMS prepolymer and curing agent (10:1 ratio) is poured over the template, cured at 65 °C for 6 h, and peeled away to reveal the microchannel. Ports are cored into the PDMS for the electrical and fluidic connections. The substrate and PDMS microfluidic layer are irreversibly bonded after O_2 plasma treatment (step g) in a diener benchtop barrel plasma RIE. Immediately following plasma activation, precise alignment of the PDMS channel to the electrodes is performed in a Carl Suss MJB3 mask aligner (step h). Figure 4i shows the top view of a cut-section of the complete microfluidic device with embedded interdigitated electrodes inside the PDMS microchannel.

3.2 Sample preparation and experimental setup

All separation experiments were performed using 0.75 μm beads (Thermo Scientific), with surface carboxylic groups that stabilized the suspension. Low conductive solutions were prepared by suspending the particles in Millipore® deionized (DI) water, and the high salt buffer was made using 0.01X PBS for an ionic strength of 1.5 mM. In both cases, the concentration of the colloids was ca. 10^7 particles per mL and the suspensions were agitated prior to each experiment. During the separation experiment, the colloids were fed into the microfluidic chip through two inlet channels at ≤30 nL/min using a syringe pump (Harvard Apparatus). Each pair of electrodes was electrically biased by a signal generator (Agilent 33250). Both the function generators were coupled through the external 10 MHz timebase, and the waveforms were synchronized in-phase using the internal triggering capability. The additional DC offset was applied for one pair of

electrodes to create the transverse DC bias. Particle flow and separation in the microchannel was optically imaged (Nikon FN-1 fluorescence microscope) with high-NA objective.

4 Results and discussion

Separation experiments were performed with the microfluidic device with two arrays of interdigitated electrodes, using 0.75 μm diameter particles in DI water that served as a low conductive medium. Figure 5 shows a series of time lapse snapshots of the colloidal particles getting collected between the 5 μm wide electrodes when a 2 V_{PP} 1 MHz AC signal was used. The transverse DC bias across the microchannel between the top and bottom electrode pairs was +1 V. Upon biasing the system, we observed particles gradually getting trapped over the top electrode pair and near the tips of the bottom electrodes. Some of the particles from the channel gap were also captured. Within about 60 s of applying the AC/DC bias, the colloids had redistributed themselves to the collection zones.

The colloid separation profile across the microchannel has also been analyzed in Fig. 6. As shown in Fig. 6a, the two cross-sections of interest are directly over the electrodes (AA') and through the midline of the electrode spacing (BB'). The mean grey values of the background before the separation experiment (blue) and after t=60 s of separation (red) have been superimposed for both these cross-sections in Fig. 6b and c, respectively. Due to the AC frequency of this experiment, we observed that the colloids preferentially accumulated in the electrode gaps and the grey values also reflect this trend. The local minima in the red curves follow the occurrence of the colloidal particle (dark) and, hence, the gray value is lower in these collection zones. More colloids are collected at the top electrodes and the tips of the bottom electrodes as seen by the grey value distributions. While the gray values in the bulk region overlapped, as expected, a few local minima are also indicative of the instantaneous occurrence of some of the particles in flow. The difference in grey values between separation and background for the BB' cross-section within the electrode pairs has been used to determine the relative particle concentration of each snapshot. When this difference is statistically significant, it indicates the presence of a particle. By averaging this over all points along the length of the electrodes, we obtain the relative concentration as a percentage. This is plotted for the electrode regions of each snapshot in Fig. 6d. As seen in Fig. 6d, the particle concentration increases over time until 71 % at t=30 s and saturates to ca. 75 % by t=60 s.

Incorporating the additional transverse DC bias enables the electric field to penetrate fully across the channel for improved capture of the colloidal particles from the bulk region. We compared this case against conventional DEP by applying only the AC bias (in-phase) at both pairs of electrodes. Figure 7 shows time lapse snapshots (t=0, 10, 30 and 60 s) of colloid separation with +1 V DC bias (Fig. 7a) and without DC bias (Fig. 7b). The AC bias used was 10 V_{PP} and 100 kHz at which we can expect positive DEP effects. The relative particle concentrations are also plotted for both cases over the electrode (Fig. 7c) and bulk (Fig. 7d) regions. As seen from the time lapse sequence of Fig. 7a, the presence of a transverse DC bias greatly improved the capture from the bulk region outside the electrodes and almost all of the particles were trapped by t=60 s. This is also consistent with the increase in concentration over the electrodes to 83 % (Fig. 7c) and decrease from 30 % to zero in the bulk region (Fig. 7d). In contrast, the AC-only case (Fig. 7b) showed particle trapping only over the electrodes (Fig. 7c). The bulk region was largely unaffected, as seen in Fig. 7d, except for minimal extraction (ca. 58 %) from the fringing regions at the electrode tips. The electric fields were localized over the electrodes and did not sufficiently extend out across the microchannel.

Further, the effect of salt concentration is analyzed by comparing with a high salt medium (0.01X PBS) in Fig. 8. The separation results were obtained at t= 60 s in both cases, with an applied AC bias of 10 V_{PP} along with the transverse +1 V DC bias between the top and bottom electrode pairs. Figure 8a shows the

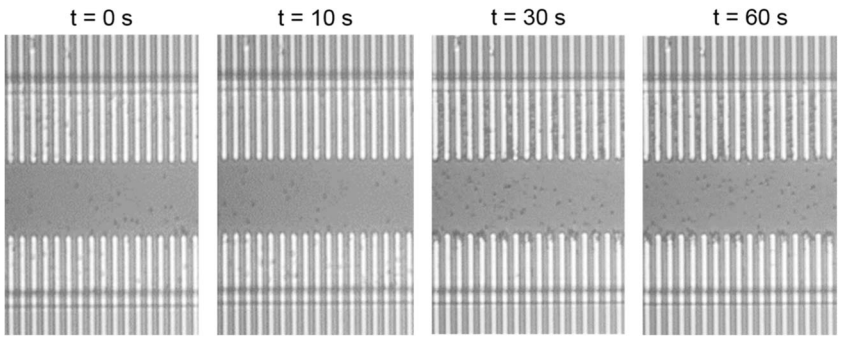

Fig. 5 Sequential snapshots of colloid separation (0.75 μm particles) using 2 V_{PP} and 1 MHz AC bias on each electrode pair, with + 1 V DC bias for the top electrodes. Images were extracted after turning on voltages at t=0, 10, 30 and 60 s, respectively, and show progressive increase in the collection of the electrodes

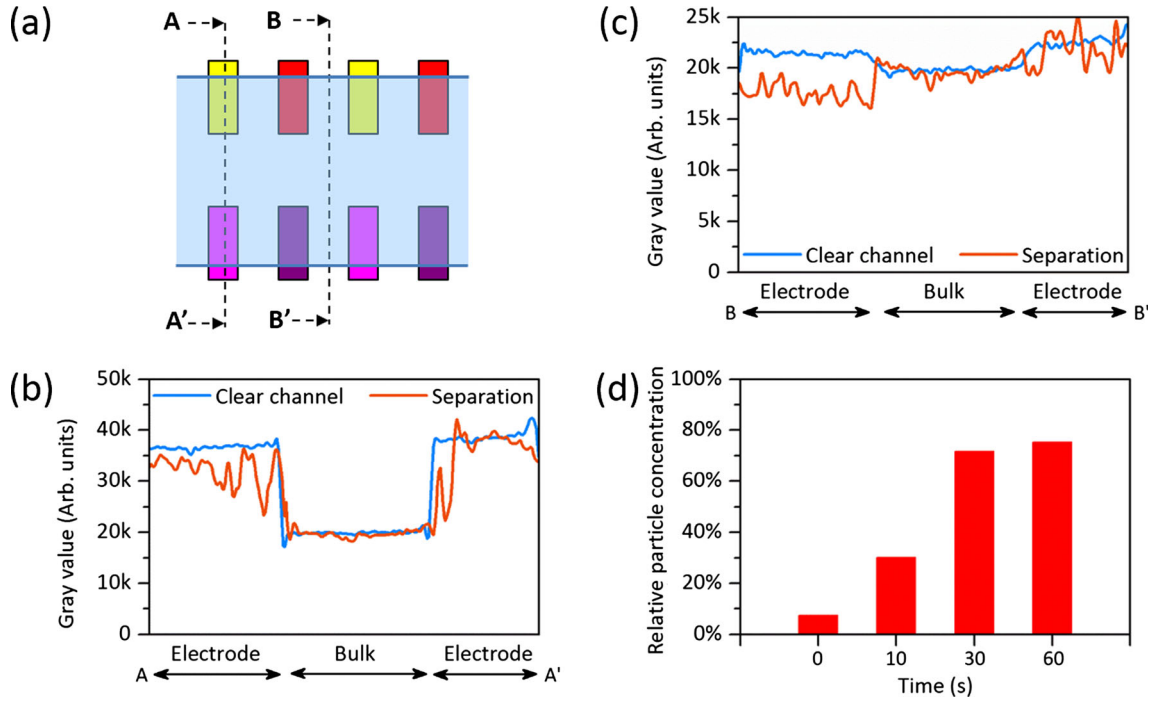

Fig. 6 Mean *gray* value profiles across the channel for particle distribution comparing collected particles and background. **a** Schematic cross-sections AA' (overlapping the electrodes) and BB' (in-between electrode gap) that were analyzed across the channel. **b** Profile through section AA' on top of electrodes. **c** Profile through section BB' over the gap between the electrodes. **d** Relative particle concentration profiles near the electrodes determined from time lapse images by subtracting gray values from background shows increasing separation with time

result for low conductive case (DI water) at 100 kHz and this is identical with the t=60 s snapshot from Fig. 7a. The particles travelled towards the electrodes and were fully captured from the bulk as well due to the transverse electric field. The particle concentration data (Fig. 8c) also shows high accumulation at the

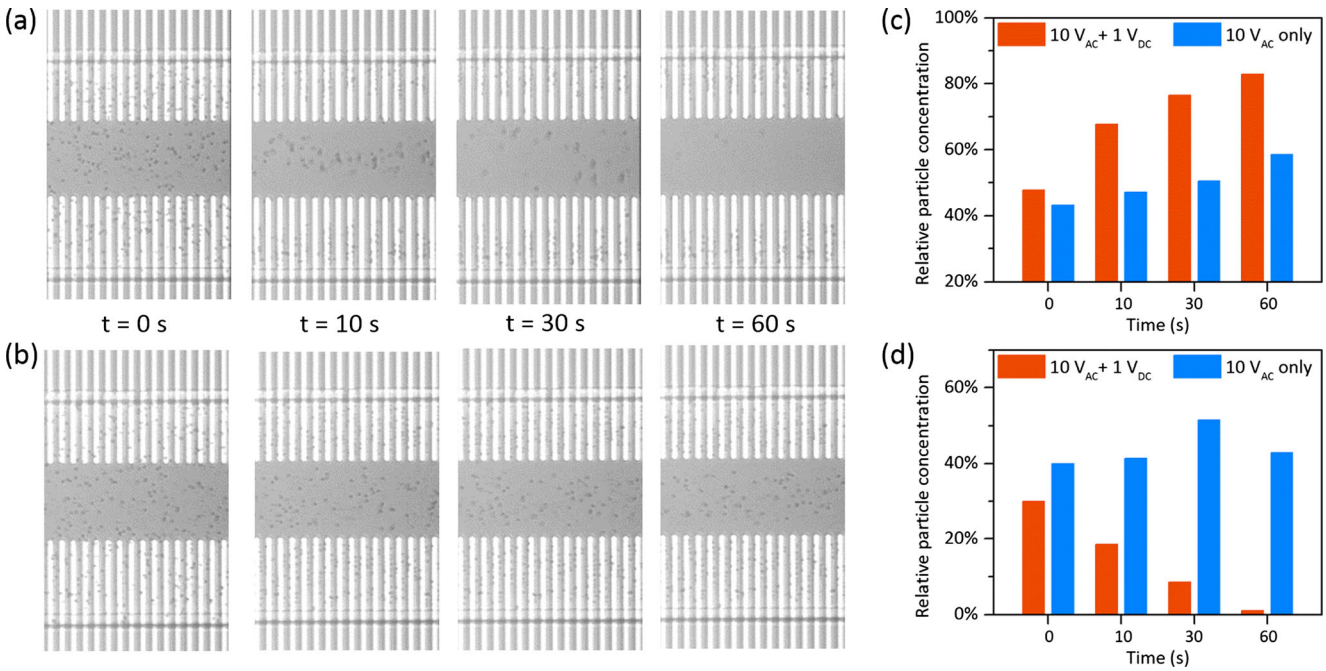

Fig 7 Sequential snapshots of colloid separation (0.75 μm particles) showing **a** with and **b** without the 1 V DC transverse bias. A higher 10 V_{PP} and 100 kHz AC bias was applied at each electrode pair. **a** Including the transverse DC bias enabled capture of the colloids from the bulk stream, whereas **b** in the AC-only case, the fields were localized over the electrodes and the bulk stream was unaffected. Relative particle concentration determined from mean gray values of cross-section profiles at both **c** electrode and **d** bulk regions confirmed this trend

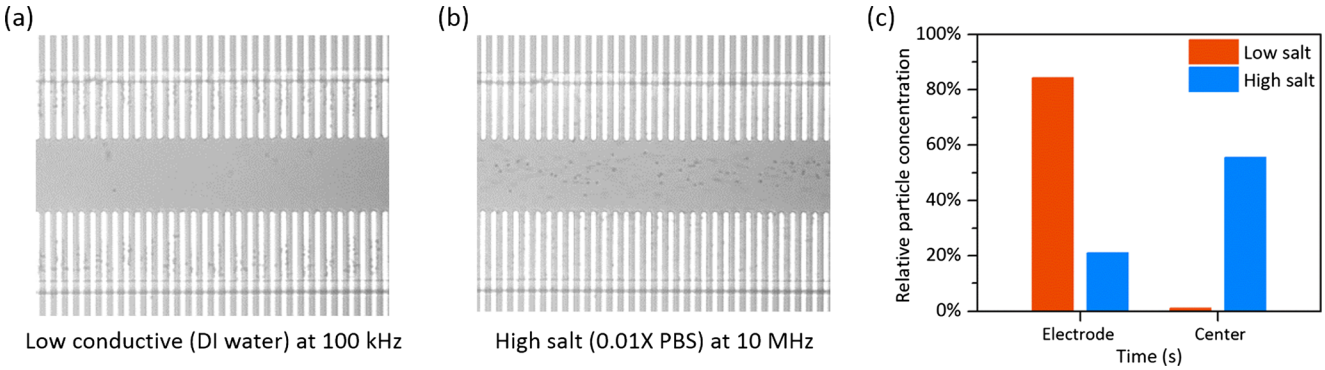

Fig. 8 Comparison of colloid separation profiles at t=60 s between low and high conductivity solutions. The signal used was 10 V_{PP} AC bias and 1 V_{DC} transverse bias, with AC frequencies selected based on the ionic strengths. **a** Low salt (DI water) at 100 kHz shows nearly complete capture, including from the bulk region. **b** High salt (0.01X PBS~ 1.5 mM) at 10 MHz shows only local particle collection by the electrodes and the bulk particles focusing to a narrow stream along the centerline. **c** Relative particle concentration at both electrode and bulk regions determined from gray values of cross-section profiles

electrodes (83 %) and complete depletion from the center regions of the microchannel. At high salt content of ca. 1.5 mM in the case of 0.01X PBS at 10 MHz, however, the high conductivity of the medium competes with the polarizability of the particle and hence Re(K(ω))<0 throughout the frequency spectrum. As a result, the colloidal particles can only experience negative DEP forces, which was apparent in Fig. 8b. The relative particle concentration (Fig. 8c) at the electrodes was 4-fold lower (21 %) and it increased to over 50 % in the bulk region. We observed that the colloids aggregated at the edges of the electrodes and those in the bulk region of the channel were repelled away towards the centerline of the channel and focused into a narrower stream.

5 Conclusions

Dielectrophoretic capture of particles is strongly dependent on the relative polarizability of the particles, as well as the scaling of electric fields relative to the particle size and characteristic microfluidic dimensions. Capture schemes will greatly benefit from the ability to enhance the electric fields through the use of interdigitated microelectrode arrays. At the same time, combining a high frequency AC depolarization with transverse DC bias across the separation zone enhances the forces of separation acting on the particles. Our results have indicated that the mixed biasing scheme provides the ability to sustain electric fields in bulk to improve the capture of sub-micron colloidal particles that are normally less affected by electrostatic separation forces. Our method can be used to spatially design the electrostatic separation schemes with improved efficiency as well as particle collection systems with discrete, well-defined collection zones for targeted capture.

Acknowledgments The authors would like to thank Dr. Bruce Flachsbart for assistance in microfabrication, Dr. Glennys Mensing for assistance with microfluidics, and Dr. Bobby Reddy (Jr.) and Dr. Eric Salm for useful discussions. Microfabrication facilities were provided by the Micro-Nano Mechanical Systems Laboratory and Micro and Nanotechnology Laboratory at UIUC. This research was financially supported through the National Institutes of Health (R01CA20003) and the US Defense Advanced research Projects Agency (W911NF09C0079).

Appendix

The nature and extent of DEP forces (attractive/repulsive) is determined by the relative polarizability of the particles over the background medium. This is characterized from the material properties by the Clausius-Mossotti factor, $K(\omega)$, which is determined as follows:

$$K(\omega) = \frac{\varepsilon_p^* - \varepsilon_m^*}{\varepsilon_p^* + 2\varepsilon_m^*} \quad (4)$$

where, $\varepsilon^* = \varepsilon + \frac{\sigma}{j\omega}$ is the complex permittivity, and the subscripts p and m represent the particle and medium respectively. K(ω) appears as a scaling coefficient in the calculation of $<F_{DEP}>$ and is bounded as follows: $-0.5<\mathrm{Re}(K(\omega))<1$ for DEP and $-1<\mathrm{Im}(K(\omega))<0$ for twDEP for homogenous spherical particles. Figure 9 shows plots of the real and imaginary components of (K(ω)) for polystyrene beads (ε_r=2.6) in aqueous solutions (ε_r=80) across the frequency spectrum for various background ionic strengths.

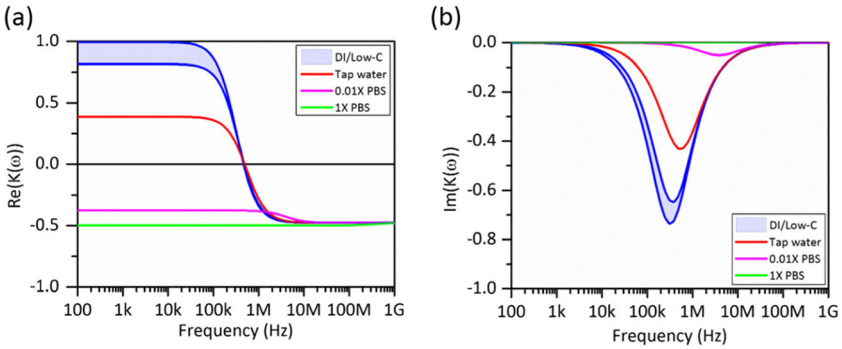

Fig. 9 Clausius-Mossotti factor calculations showing the response of colloidal beads to DEP forces. **a** Real and **b** Imaginary components of (K(ω)) vs. AC frequency shows predominantly nDEP response

References

D.R. Albrecht, R.L. Sah, S.N. Bhatia, Biophys. J. **87**, 2131 (2004)

P. Bajaj, D. Marchwiany, C. Duarte, R. Bashir, Adv. Healthc. Mater. **2**, 450 (2013)

A.J. Bard, L.R. Faulkner, *Electrochemical methods: fundamentals and applications*, 2nd edn. (Wiley, New York, 2001)

M.Z. Bazant, T.M. Squires, Curr. Opin. Colloid Interface Sci. **15**, 203 (2010)

J. Cao, P. Cheng, F. Hong, J. Electrost. **66**, 620 (2008)

A. Castellanos, A. Ramos, A. González, N.G. Green, H. Morgan, J. Phys. Appl. Phys. **36**, 2584 (2003)

J. Čemažar, D. Vrtačnik, S. Amon, T. Kotnik, IEEE Trans. NanoBiosci. **10**, 36 (2011)

E.G. Cen, C. Dalton, Y. Li, S. Adamia, L.M. Pilarski, K.V.I.S. Kaler, J. Microbiol. Methods **58**, 387 (2004)

B. Edwards, A. Timperman, R. Carroll, K. Jo, J. Mease, and J. Schiffbauer, Phys. Rev. Lett. **102**, (2009).

N. Gadish, J. Voldman, Anal. Chem. **78**, 7870 (2006)

P.R.C. Gascoyne, J. Vykoukal, Electrophoresis **23**, 1973 (2002)

T. Horii, M. Yamamoto, T. Yasukawa, F. Mizutani, Biosens. Bioelectron. **61**, 215 (2014)

C. Huang, H. Liu, N.H. Bander, B.J. Kirby, Biomed. Microdevices **15**, 941 (2013)

K.D. Jo, J.E. Schiffbauer, B.E. Edwards, R. Lloyd Carroll, A.T. Timperman, Analyst **137**, 875 (2012)

W. Li, H. Du, D. Chen, C. Shu, Comput. Mater. Sci. **30**, 320 (2004)

H. Li, Y. Zheng, D. Akin, R. Bashir, J. Microelectromech. Syst. **14**, 103 (2005)

D. Liu, S.V. Garimella, Nanoscale Microscale Thermophys. Eng. **13**, 109 (2009)

K. Park, D. Akin, R. Bashir, Biomed. Microdevices **9**, 877 (2007)

K. Park, H.-J. Suk, D. Akin, R. Bashir, Lab Chip **9**, 2224 (2009)

A. J. Pascall and T. M. Squires, Phys. Rev. Lett. **104**, (2010).

R. Pethig, Biomicrofluidics **4**, 022811 (2010)

H.A. Pohl, *Dielectrophoresis: the behavior of neutral matter in nonuniform electric fields* (Cambridge University Press, Cambridge, 1978)

E.D. Pratt, C. Huang, B.G. Hawkins, J.P. Gleghorn, B.J. Kirby, Chem. Eng. Sci. **66**, 1508 (2011)

A. Ramos, H. Morgan, N.G. Green, A. Castellanos, J. Colloid Interface Sci. **217**, 420 (1999)

T. Sun, H. Morgan, and N. Green, Phys. Rev. E **76**, (2007).

L. Wang, J. Lu, S.A. Marchenko, E.S. Monuki, L.A. Flanagan, A.P. Lee, Electrophoresis **30**, 782 (2009)

J. Wu, J. Appl. Phys. **103**, 024907 (2008)

J.D. Yantzi, J.T.W. Yeow, S.S. Abdallah, Biosens. Bioelectron. **22**, 2539 (2007)

T. Yasukawa, H. Hatanaka, F. Mizutani, Anal. Chem. **84**, 8830 (2012)

H. Zhou, L.R. White, R.D. Tilton, J. Colloid Interface Sci. **285**, 179 (2005)

K. Zhu, A.S. Kaprelyants, E.G. Salina, G.H. Markx, Biomicrofluidics **4**, 022809 (2010)